Small Signal Modeling and Transient Cross-Regulation Analysis of Peak-Current-Mode-Controlled SIDO Buck LED Driver

Yao Wang, Jianping Xu, *Member, IEEE*, Zhangyong Chen, and Fuban Qin

***Abstract*—Single-inductor dual-output (SIDO) dc–dc converter has been applied to light-emitting diode (LED) drivers with its advantages of small volume and low cost. Peak-current-mode (PCM) control of the SIDO converter has the advantages of fast transient performance and suppressed cross-regulation. A PCM-controlled SIDO buck LED driver to achieve independent dimming and to eliminate the steady-state cross-regulation is proposed in this article. The circuit and the principle of the PCM-controlled SIDO buck LED driver are presented, and its small signal model is established based on inductor current ripple. Furthermore, based on control-to-output loop gain transfer functions, control parameters of PCM-controlled SIDO buck LED driver are designed to achieve independent output current regulation of each LED driver. Besides, cross-regulation transfer functions are obtained to investigate the effect of reference signals and control parameters on the transient cross-regulation. Moreover, the effect of capacitor parameters on the stability of the LED driver is analyzed based on the bifurcation diagram. Finally, experimental results are provided to show the independent dimming capability of PCM-controlled SIDO buck LED driver with designed parameters, and the validity of the theoretical analysis on transient cross-regulation and stability of the LED driver.**

***Index Terms*—Light-emitting diode (LED) driver, peak-current-mode (PCM), single-inductor dual-output (SIDO), small signal model, transient cross-regulation.**

NOMENCLATURE

v_i	Input voltage.
C_1, C_2	Output capacitors of output 1 and output 2.
i_1, i_2	Output currents of output 1 and output 2.
v_1, v_2	Output voltages of output 1 and output 2.
R_{d1}, R_{d2}	Equivalent resistors of LED_1 and LED_2.
V_d	Forward voltages of LED_1 and LED_2.
T	Switching cycle.
r_s	Sensed resistor of inductor current.
r_{s1}, r_{s2}	Sensed resistors of output current i_1 and i_2.
V_{g1}, V_{g2}	Control signals of power switch S_1 and S_2.
d_1, d_2	Duty cycles of control signal V_{g1} and V_{g2}.
i_{ref1}, i_{ref2}	Reference signals of output current i_1 and i_2.
v_{c1}, v_{c2}	Amplified error voltages by PI_1 and PI_2.
k_1, k_2, k_3	Inductor current slopes in switch mode I, II, and III.
k_{p1}, k_{i1}	Proportional and integral coefficients of PI_1.
k_{p2}, k_{i2}	Proportional and integral coefficients of PI_2.
A_j, B_j	Coefficient matrixes of the state equation.
$\mathbf{A}$, $\mathbf{B}$	Coefficient matrixes of the state-space averaging model.
$\hat{i}_L$	Small signal variable of inductor current.
$\hat{i}_1$, $\hat{i}_2$	Small signal variables of output current.
$\hat{v}_1$, $\hat{v}_2$	Small signal variables of output voltage.
$\hat{d}_1$, $\hat{d}_2$	Small signal variables of duty cycle.
$\hat{i}_{\text{ref1}}$, $\hat{i}_{\text{ref2}}$	Small signal variables of reference signal.
$G_{\hat{i}_1/\hat{d}_1}(s)$	Open-loop control-to-output transfer function of output 1 (d_1 to i_1).
$G_{\hat{i}_2/\hat{d}_2}(s)$	Open-loop control-to-output transfer function of output 2 (d_2 to i_2).
$G_{\hat{i}_L/\hat{d}_1}(s)$	Open-loop control-to-inductor current transfer function (d_1 to i_L).
$G_{\hat{i}_L/\hat{d}_2}(s)$	Open-loop control-to-inductor current transfer function (d_2 to i_L).
$G_{\hat{d}_1/\hat{i}_{\text{ref1}}}(s)$	Reference-to-control transfer function of output 1 ($\hat{i}_{\text{ref1}}$ to $\hat{d}_1$).
$G_{\hat{d}_2/\hat{i}_{\text{ref2}}}(s)$	Reference-to-control transfer function of output 2 ($\hat{i}_{\text{ref2}}$ to $\hat{d}_2$).
$G_{\hat{d}_1/\hat{i}_L}(s)$	Inductor current-to-control transfer function ($\hat{i}_L$ to $\hat{d}_1$).
$G_{\hat{d}_2/\hat{i}_L}(s)$	Inductor current-to-control transfer function ($\hat{i}_L$ to $\hat{d}_2$).

Manuscript received 14 February 2023; revised 12 May 2023; accepted 24 June 2023. Date of publication 6 July 2023; date of current version 1 September 2023. This work was supported in part by the National Nature Science Foundation of Sichuan Province under Grant 2022NSFSC1913, and in part by the Fundamental Research Funds for the Central Universities, Southwest Minzu University under Grant 2021101. Recommended for publication by Associate Editor F. Azcondo. *(Corresponding author: Yao Wang.)*

Yao Wang is with the School of Electrical Engineering, Southwest Minzu University, Chengdu 610041, China (e-mail: wangyao_zoe@foxmail.com).

Jianping Xu is with the School of Electrical Engineering, Southwest Jiaotong University, Chengdu 611756, China, and also with the Key Laboratory of Magnetic Suspension Technology and Maglev Vehicle, Ministry of Education, Chengdu 611756, China (e-mail: jpxu-swjtu@163.com).

Zhangyong Chen is with the School of Automation Engineering, University of Electronic Science and Technology of China, Chengdu 611731, China (e-mail: zhang_yong_ch@126.com).

Fuban Qin is with Texas Instruments (Chengdu), Chengdu 611731, China (e-mail: fuban_qin@163.com).

Color versions of one or more figures in this article are available at https://doi.org/10.1109/TPEL.2023.3292906.

Digital Object Identifier 10.1109/TPEL.2023.3292906

$G_{\hat{d}_1/\hat{i}_1}(s)$	Output-to-control transfer function of output 1 ($\hat{i}_1$ to $\hat{d}_1$).
$G_{\hat{d}_1/\hat{i}_2}(s)$	Output-to-control transfer function of output 2 ($\hat{i}_2$ to $\hat{d}_1$).
$G_{\hat{d}_2/\hat{i}_1}(s)$	Output-to-control transfer function of output 1($\hat{i}_1$ to $\hat{d}_2$).
$G_{\hat{d}_2/\hat{i}_2}(s)$	Output-to-control transfer function of output 2 ($\hat{i}_2$ to $\hat{d}_2$).
$T_1(s)$	Control-to-output loop gain transfer function of output 1 ($\hat{d}_1$ to $\hat{i}_1$).
$T_2(s)$	Control-to-output loop gain transfer function of output 2 ($\hat{d}_2$ to $\hat{i}_2$).
$G_{\hat{i}_1/\hat{i}_{\rm ref2}}(s)$	Cross-regulation transfer function of output 1 ($\hat{i}_{ref2}$ to $\hat{i}_1$).
$G_{\hat{i}_2/\hat{i}_{\rm ref1}}(s)$	Cross-regulation transfer function of output 2 ($\hat{i}_{\rm ref1}$ to $\hat{i}_2$).
f_c	Cross-over frequency of $T_1(s)$ and $T_2(s)$.
Δi_1, Δi_2	Output current ripples of i_1 and i_2.

I. Introduction

COMPARED with other illumination types, light-emitting diode (LED) has the advantages of high efficiency, long lifetime, flexible color mixing, and energy saving. Therefore, LED has been widely used in the lighting industry, such as general lighting, decorative lighting, vehicle lighting, display backlighting, and so on [1], [2]. Due to the power limitation of a single LED, series/parallel configuration LED string are usually utilized to extend the power range to meet the requirement of high-power applications. A typical parallel configuration of an LED driver with independent-converter architecture, as shown in Fig. 1, is widely used due to its advantage of constant and independent current regulation of each LED string [3], [4], [5]. However, such a parallel configuration increases the circuit volume and the cost due to the extra components, such as inductors and switches, thus decreases the power density of the LED driver.

For the LED driver of parallel LED string, it is important to reduce its volume and cost [6], [7], [8]. Single-inductor multiple-output (SIMO) converter with only one inductor has been used in portable devices. It can provide multiple outputs with small circuit volume and low cost. SIMO converter has also attracted much attention in multiple-output LED drivers. The system architecture of the SIMO LED driver is shown in Fig. 2, which is simple, and the number of inductors is significantly decreased.

SIMO converter has three operation modes: discontinuous conduction mode (DCM), pseudocontinuous conduction mode (PCCM), and continuous conduction mode (CCM). The DCM SIMO converter usually operates in light load due to the large current and voltage ripple in heavy load. The CCM SIMO converter can achieve low ripple and high efficiency. However, as one inductor is shared by multiple outputs, load variation of one output of the CCM SIMO converter may cause steady-state and transient cross-regulation on other outputs [9]. The PCCM SIMO converter is implemented to overcome the shortcoming of DCM SIMO converter and CCM SIMO converter. However,

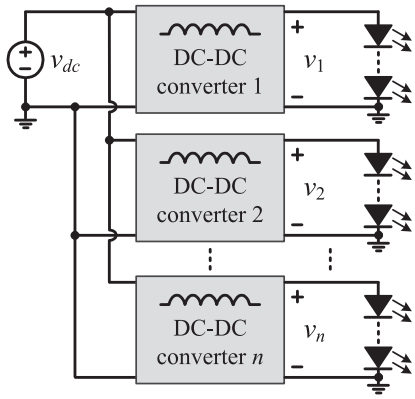

Fig. 1. System architecture of a traditional multiple-output LED driver.

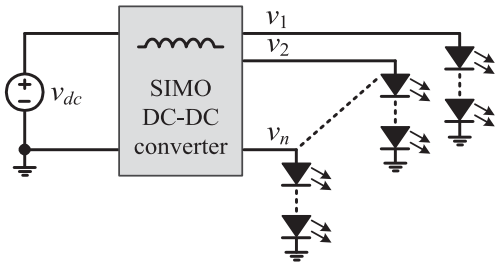

Fig. 2. System architecture of a single-inductor multiple-output LED driver.

the PCCM SIMO converter suffers reduced efficiency due to an additional freewheeling switch [10]. Up to now, only DCM and CCM SIMO converters have been applied to the multiple-output LED driver, in which ripple and cross-regulation issues still exist for the SIMO LED driver.

The time-multiplexing (TM) scheme has been widely applied to the DCM SIMO LED driver. The average current mode control with a TM scheme for a SIMO boost LED driver is proposed in [1]. This scheme optimizes local bus voltage for power loss reduction and offers flexible dimming for backlighting operations. A quasi-hysteretic finite-state-machine-based digital control with a TM scheme is used for a single-inductor dual-output (SIDO) buck LED driver, which reduces the complexity of the controller design by eliminating loop compensation, and can drive more LED strings without limit by the maximum LED current rating [8]. A capacitor-free SIDO LED driver with integrated laterally double-diffused metal-oxide semiconductor (LDMOS) is addressed in [11], which shows the excellent characteristics of the LDMOS in the SIMO application. In these studies, a single time-shared control loop is employed for average current regulation in multiple parallel LED strings, resulting in current balance error and steady-state cross-regulation.

A single-stage ac/dc SIMO LED driver in DCM is proposed in [3], which presents the voltage mode (VM) control with a TM scheme to achieve a high power factor and independent current control of each LED string. In addition, the independent VM–TM control for each LED string eliminates the steady-state cross-regulation. However, the inductor current ripple and the output current ripple are serious. Based on coordinating a string-level scheme and a system-level dimming scheme, a DCM SIMO

buck LED driver is proposed to improve dimming precision and extend the dimming range [4]. The steady-state cross-regulation is also eliminated with independent control. Nevertheless, the dimming switches inserted in individual LED channels result in overshoot current and low efficiency.

To improve the efficiency and to suppress the steady-state cross-regulation, the average current correction technique with TM for the CCM SIMO buck LED driver is presented in [12]. A TM control CCM SIMO boost LED driver is proposed to drive multiple channel LEDs with equal currents and brightness for display backlight applications [13]. It is worth noting that the mentioned driver does not utilize serially inserted current regulation elements in individual LED channels, thus it has high efficiency. A CCM SIMO LED driver is applied for a three-color LED lighting system [6]. The average current control technique independently controls the LED driver, which has small steady-state cross-regulation. A current-source-mode SIMO LED driver with a single voltage control loop is proposed to have an independent dimming function and to eliminate steady-state cross-regulation [14]. In these studies, although the steady-state cross-regulation is eliminated, the dimming control of each LED string results in interference in the average current of different LED strings. Thus, the LED driver still exists in transient cross-regulation.

The research for CCM SIMO converter shows that the transient cross-regulation can be suppressed by digital control [15], [16], decouple control [17], [18], and ripple-based control techniques [9], [19]. However, digital control and decouple control techniques require a considerable computation burden, while the ripple-based control techniques, which have a fast transient response and simple structure, can significantly suppress the transient cross-regulation. Current-mode dual-loop ripple control is proposed to suppress transient cross-regulation for the SIDO boost converter under different inductor current trends and switch sequences [20]. It shows that peak-current-mode (PCM) control is one of the ripple-based control techniques with advantages of simple structure, fast transient performance, and reduced cross-regulation.

In view of the aforementioned issues, this article designs a parallel LED string driver for the SIDO buck LED driver with PCM control. The proposed PCM-controlled LED driver has the advantages of small volume and low cost due to the reduced number of inductors. With two independent PCM control loops, the independent dimming capability is achieved to eliminate the steady-state cross-regulation. The inductor current operates in CCM. Thus, the driver has a small ripple. In addition, the small signal model of the PCM-controlled SIDO buck LED driver is established for the design of control parameters and for the analysis of the transient cross-regulation. The effect of the transient cross-regulation with different reference signals i_{ref2} and control parameters k_{p1} and k_{p2} of this LED driver are summarized. Furthermore, the effect of capacitor parameters on the stability and the efficiency of this LED driver is analyzed.

The paper is organized as follows. Section II presents the circuit configuration and the operation principle of the PCM-controlled SIDO Buck LED driver. Section III investigates the small signal model, control-to-output loop gain transfer functions, and cross-regulation transfer functions of the PCM-controlled SIDO Buck LED driver. Besides, the design of the control parameters and the analysis of the transient cross-regulation based on these transfer functions are presented. Based on the bifurcation diagram, the effect of capacitor parameters on the stability of this LED driver is analyzed. Section VI gives experimental results to demonstrate theoretical analysis, followed by the conclusion in Section V.

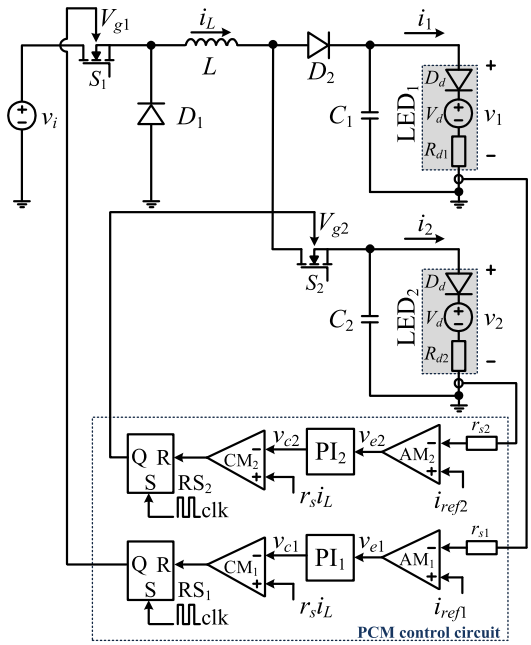

Fig. 3. Circuit configuration of a PCM-controlled SIDO buck LED driver.

II. PCM-Controlled SIDO Buck LED Driver

A. Circuit Configuration

The circuit configuration of the PCM-controlled SIDO buck LED driver is shown in Fig. 3, including the power stage circuit and PCM control circuit. The power stage circuit consists of an input voltage source v_i, an inductor L, two power switches S_1 and S_2, two diodes D_1 and D_2, two capacitors C_1 and C_2, and two LED strings LED$_1$ and LED$_2$, which are, respectively, equivalent to a series connection of an ideal diode D_d, a voltage source with forward voltage V_d, and an equivalent resistor R_{d1} or R_{d2} [2]. It should be noted that the mentioned components are ideal to simplify the analysis.

The two LED strings are regarded as output 1 and output 2 of the LED driver with output currents of i_1 and i_2. To guarantee the conduction of the power switch S_2 and diode D_2 are complementary, i.e., when S_2 is turned ON, D_2 is turned OFF, it should have $i_1 > i_2$. When the diode D_2 is replaced by a power switch S, the studied LED driver can operate normally at any conditions of $i_1 > i_2$, $i_1 < i_2$, and $i_1 = i_2$. However, it requires a driver circuit of the power switch S and a NOT gate, which increases the LED driver's cost and volume.

The PCM control circuit is composed of two PCM control loops with an inductor current sensed resistor r_s, two output

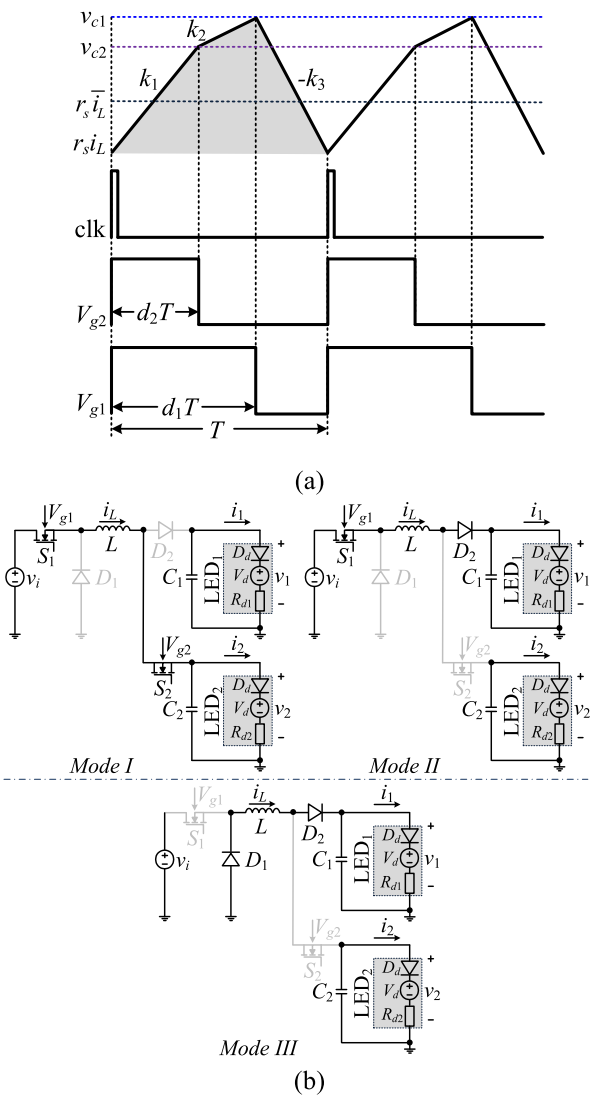

Fig. 4. Control timing and operating modes of the PCM-controlled SIDO buck LED driver. (a) Control timing. (b) Operating modes.

current sensed resistors r_{s1} and r_{s2}, two amplifiers AM_1 and AM_2, two PI regulators PI_1 and PI_2, two comparators CM_1 and CM_2, two RS triggers RS_1 and RS_2, and one clock signal clk. Control signals V_{g1} and V_{g2} are generated by these two control loops. Duty cycles d_1 and d_2 correspond to V_{g1} and V_{g2}. Power switch S_1 and diode D_1 are used to control the input power by adjusting duty cycle d_1. Power switch S_2 and diode D_2 are used to control the power distribution from input to two outputs by adjusting duty cycle d_2.

B. Operation Principle

Fig. 4(a) shows the control timing of the PCM-controlled SIDO buck LED driver with $d_1 > d_2$. As shown in Figs. 3 and 4(a), power switches S_1 and S_2 are turned ON by clk signal at the beginning of each switching cycle, and sensed inductor current $r_s i_L$ increases linearly with the slope of k_1. The output currents i_1 and i_2 are sampled by sensed resistors r_{s1} and r_{s2}, and compared with reference signals of i_{ref1} and i_{ref2} to generate error voltages of v_{e1} and v_{e2} by using AM_1 and AM_2, respectively. These error voltages are amplified and compensated by PI_1 and PI_2 to generate control voltages v_{c1} and v_{c2}. Then, $r_s i_L$ is compared with v_{c1} and v_{c2} by CM_1 and CM_2, respectively, to generate turn-OFF signals of power switches S_1 and S_2, i.e., when $r_s i_L$ increases to v_{c2}, S_2 is turned OFF and $r_s i_L$ keeps increasing linearly with the slope of k_2. In contrast, when $r_s i_L$ increases to v_{c1}, S_1 is turned OFF and $r_s i_L$ decreases linearly with the slope of k_3.

Fig. 4(b) shows three operating modes corresponding to this control timing as follows:

Mode I: Power switches S_1 and S_2 are turned ON, and diodes D_1 and D_2 are turned OFF. Sensed inductor current $r_s i_L$ increases with the slope k_1.

Mode II: Power switch S_2 is turned OFF, D_2 is turned ON, S_1 keeps ON, and D_1 keeps OFF. Sensed inductor current $r_s i_L$ increases with the slope k_2.

Mode III: Power switch S_2 is turned OFF, diode D_2 is turned ON, S_1 keeps OFF, and D_1 keeps ON. Sensed inductor current $r_s i_L$ decreases with the slope $-k_3$ until the beginning of the next switching cycle.

The slopes k_1, k_2, and k_3 are given as follows:

$$\begin{aligned} k_1 &= (v_i - V_d - R_{d2} i_2)/L, \\ k_2 &= (v_i - V_d - R_{d1} i_1)/L, \\ k_3 &= (V_d + R_{d1} i_1)/L. \end{aligned} \tag{1}$$

III. Small Signal Modeling for PCM-controlled SIDO Buck LED Driver

In order to design control parameters and to investigate the transient cross-regulation of the PCM-controlled SIDO buck LED driver, a small signal model of the studied driver is established.

A. Small Signal Modeling for SIDO Buck LED Driver

Defining the state variable vector of SIDO buck LED driver as $\boldsymbol{x} = [i_L v_1 v_2]^{\mathrm{T}}$ and the input variable vector as $\boldsymbol{v} = [v_i v_d]^{\mathrm{T}}$, where v_1 and v_2 denote the output voltages of LED_1 and LED_2, respectively. The state equation of the SIDO buck LED driver for each operating mode is given as follows:

$$\dot{\mathbf{x}} = \begin{cases} \mathbf{A}_1\mathbf{x} + \mathbf{B}_1\mathbf{v}, nT \le t < nT + d_2T \\ \mathbf{A}_2\mathbf{x} + \mathbf{B}_2\mathbf{v}, nT + d_2T \le t < nT + d_1T \\ \mathbf{A}_3\mathbf{x} + \mathbf{B}_3\mathbf{v}, nT + d_1T \le t < (n+1)T \end{cases} \tag{2}$$

Where T is the switching cycle; d_2T, $(d_1 - d_2)T$, and $(1 - d_1)T$ are the durations of switch mode I, II, and III, respectively. The coefficient matrixes A_j and B_j $(j = 1, 2, 3)$ are obtained as follows:

$$\mathbf{A}_1 = \begin{bmatrix} 0 & 0 & -\frac{1}{L} \\ 0 & -\frac{1}{R_{d1}C_1} & 0 \\ \frac{1}{C_2} & 0 & -\frac{1}{R_{d2}C_2} \end{bmatrix},$$

$$\mathbf{A}_2=\mathbf{A}_3=\begin{bmatrix}0 & -\frac{1}{L} & 0\\ \frac{1}{C_1} & -\frac{1}{R_{d1}C_1} & 0\\ 0 & 0 & -\frac{1}{R_{d2}C_2}\end{bmatrix},$$

$$\mathbf{B}_1=\mathbf{B}_2=\begin{bmatrix}\frac{1}{L} & 0\\ 0 & -\frac{1}{R_{d1}C_1}\\ 0 & -\frac{1}{R_{d2}C_2}\end{bmatrix},$$

$$\mathbf{B}_3=\begin{bmatrix}0 & 0\\ 0 & -\frac{1}{R_{d1}C_1}\\ 0 & -\frac{1}{R_{d2}C_2}\end{bmatrix}.$$

The state-space averaging model can be expressed as

$$\dot{\boldsymbol{x}}=\mathbf{A}\boldsymbol{x}+\mathbf{B}\boldsymbol{v} \tag{3}$$

where $\mathbf{A}=d_2\mathbf{A}_1-d_2\mathbf{A}_2+\mathbf{A}_3$ and $\mathbf{B}=d_1\mathbf{B}_1+\mathbf{B}_3-d_1\mathbf{B}_3$, i.e.,

$$\mathbf{A}=\begin{bmatrix}0 & -\frac{1}{L}(1-d_2) & -\frac{1}{L}d_2\\ \frac{1}{C_1}(1-d_2) & -\frac{1}{R_{d1}C_1} & 0\\ \frac{1}{C_2}d_2 & 0 & -\frac{1}{R_{d2}C_2}\end{bmatrix},$$

$$\mathbf{B}=\begin{bmatrix}\frac{1}{L}d_1 & 0\\ 0 & -\frac{1}{R_{d1}C_1}\\ 0 & -\frac{1}{R_{d2}C_2}\end{bmatrix}.$$

When small signal perturbations of $\hat{i}_L$, $\hat{v}_1$, $\hat{v}_2$, $\hat{d}_1$, and $\hat{d}_2$ are applied to the variables of the state-space averaging model in (3), the small signal model of the SIDO buck LED driver can be obtained as

$$\begin{cases}\hat{i}_L=\frac{1}{sL}[-(1-D_2)\hat{v}_1-D_2\hat{v}_2+V_i\hat{d}_1+(V_1-V_2)\hat{d}_2]\\ \hat{v}_1=\frac{1}{sC_1}[(1-D_2)\hat{i}_L-I_L\hat{d}_2-\frac{\hat{v}_1}{R_{d1}}]\\ \hat{v}_2=\frac{1}{sC_2}(D_2\hat{i}_L-\frac{\hat{v}_2}{R_{d2}}+I_L\hat{d}_2)\end{cases} \tag{4}$$

where the variables denoted with capital letter are the dc steady-state variables.

It can be known from Fig. 3 that the output variables $\hat{i}_1$ and $\hat{i}_2$ can be written as

$$\hat{i}_1=\frac{\hat{v}_1}{R_{d1}},\hat{i}_2=\frac{\hat{v}_2}{R_{d2}}. \tag{5}$$

According to (4) and (5), the block diagram of the small signal model of the SIDO buck LED driver can be established, as shown in Fig. 5, where $\hat{d}_1$ and $\hat{d}_2$ are chosen by the PCM control circuit.

B. Small Signal Modeling for PCM Controlled SIDO Buck LED Driver

As shown in Fig. 3, the control voltages v_{c1} and v_{c2} can be written as follows:

$$v_{c1}=\left(k_{p1}+\frac{k_{i1}}{s}\right)(i_{\text{ref1}}-r_{s1}i_1) \tag{6}$$

$$v_{c2}=\left(k_{p_2}+\frac{k_{i2}}{s}\right)(i_{\text{ref2}}-r_{s2}i_2) \tag{7}$$

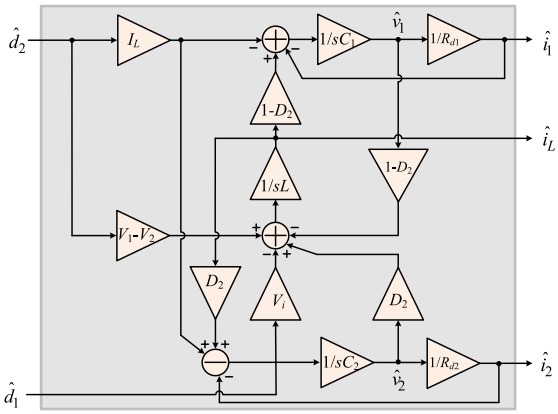

Fig. 5. Block diagram of a small signal model of SIDO buck LED driver.

where k_{p1} and k_{i1} indicate the proportional and integral coefficients of PI_1, respectively. In addition, k_{p2} and k_{i2} are the proportional and integral coefficients of PI_2, respectively.

According to the steady-state waveform of the inductor current shown in Fig. 4(a), the following relationships are obtained:

$$v_{c2}-r_si_L=k_1d_2T-r_s\bar{i}_L \tag{8}$$

$$v_{c1}-r_si_L=k_1d_2T+k_2(d_1-d_2)T-r_s\bar{i}_L \tag{9}$$

$$k_1d_2+k_2(d_1-d_2)=k_3(1-d_1) \tag{10}$$

where $r_s\bar{i}_L$ represents the average value of shadow region of r_si_L in Fig. 4(a), which is expressed by

$$r_s\bar{i}_L=\frac{T}{2}\times(k_1d_2-k_2d_2+k_2d_1+k_1d_1d_2-k_2d_1d_2+k_2d_2^2-k_1d_2^2). \tag{11}$$

Combine (8), (10), and (11), it gives

$$v_{c2}-r_si_L=\frac{T}{2(k_2+k_3)}(k_1^2d_2^2-k_1k_2d_2^2+k_1k_3d_2^2-k_2k_3d_2^2+2k_1k_2d_2+2k_2k_3d_2-k_2k_3). \tag{12}$$

Similarly, combine (9) to (11), there is

$$v_{c1}-r_si_L=\frac{T}{2(k_1-k_2)}(k_1k_2d_1^2+k_1k_3d_1^2+k_3^2d_1^2+k_2k_3d_1^2-2k_1k_3d_1-2k_3^2d_1+k_1k_3-k_2k_3+k_3^2). \tag{13}$$

From (1), (6), (7), (12), and (13), there are

$$\hat{d}_1=G_{\hat{d}_1/\hat{i}_{\text{ref1}}}(s)\hat{i}_{\text{ref1}}+G_{\hat{d}_1/\hat{i}_L}(s)\hat{i}_L+G_{\hat{d}_1/\hat{i}_1}(s)\hat{i}_1+G_{\hat{d}_1/\hat{i}_2}(s)\hat{i}_2 \tag{14}$$

$$\hat{d}_2=G_{\hat{d}_2/\hat{i}_{\text{ref2}}}(s)\hat{i}_{\text{ref2}}+G_{\hat{d}_2/\hat{i}_L}(s)\hat{i}_L+G_{\hat{d}_2/\hat{i}_1}(s)\hat{i}_1+G_{\hat{d}_2/\hat{i}_2}(s)\hat{i}_2 \tag{15}$$

where $G_{\hat{d}_1/\hat{i}_{\text{ref1}}}(s)=\frac{\alpha_1}{\delta_1}$ and $G_{\hat{d}_2/\hat{i}_{\text{ref2}}}(s)=\frac{\beta_1}{\delta_2}$ are reference-to-control transfer functions; $G_{\hat{d}_1/\hat{i}_L}(s)=\frac{\alpha_2}{\delta_1}$ and $G_{\hat{d}_2/\hat{i}_L}(s)=$

TABLE I
OPEN-LOOP TRANSFER FUNCTIONS OF THE PCM-CONTROLLED SIDO BUCK LED DRIVER

Transfer function names	Transfer functions	No.
Open-loop control-to-output transfer function ($\hat{d}_1$ to $\hat{i}_1$)	$G_{\hat{i}_1/\hat{d}_1}(s)=\frac{\hat{i}_1}{\hat{d}_1}\Big\vert_{\hat{d}_2=0}=\frac{V_i(1+sR_{d2}C_2)(1-D_2)}{(1+sR_{d1}C_1)(s^2R_{d2}LC_2+sL+R_{d2}D_2^2)+R_{d1}(1+sR_{d2}C_2)(1-D_2)^2}$	(16a)
Open-loop control-to-output transfer function ($\hat{d}_2$ to $\hat{i}_2$)	$G_{\hat{i}_2/\hat{d}_2}(s)=\frac{\hat{i}_2}{\hat{d}_2}\Big\vert_{\hat{d}_1=0}=\frac{R_{d1}I_LD_2(1-D_2)+D_2(V_1-V_2)(1+sR_{d1}C_1)+I_L\left[s^2R_{d1}LC_1+sL+R_{d1}(1-D_2)^2\right]}{(1+sR_{d2}C_2)\left[s^2R_{d1}LC_1+sL+R_{d1}(1-D_2)^2\right]+R_{d2}D_2^2(1+sR_{d1}C_1)}$	(16b)
Open-loop control-to-inductor current transfer function ($\hat{d}_1$ to $\hat{i}_L$)	$G_{\hat{i}_L/\hat{d}_1}(s)=\frac{\hat{i}_L}{\hat{d}_1}\Big\vert_{\hat{d}_2=0}=\frac{V_i(1+sR_{d2}C_2)(1+sR_{d1}C_1)}{sL(sR_{d1}C_1+1)(sR_{d2}C_2+1)+(1-D_2)^2R_{d1}(sR_{d2}C_2+1)+D_2^2R_{d2}(sR_{d1}C_1+1)}$	(17a)
Open-loop control-to-inductor current transfer function ($\hat{d}_2$ to $\hat{i}_L$)	$G_{\hat{i}_L/\hat{d}_2}(s)=\frac{\hat{i}_L}{\hat{d}_2}\Big\vert_{\hat{d}_1=0}=\frac{(1-D_2)I_LR_{d1}(sR_{d2}C_2+1)-D_2I_LR_{d2}(sR_{d1}C_1+1)+(V_1-V_2)(sR_{d1}C_1+1)(sR_{d2}C_2+1)}{sL(sR_{d1}C_1+1)(sR_{d2}C_2+1)+(1-D_2)^2R_{d1}(sR_{d2}C_2+1)+D_2^2R_{d2}(sR_{d1}C_1+1)}$	(17b)

$\frac{\beta_2}{\delta_2}$ are inductor current-to-control transfer functions; $G_{\hat{d}_1/\hat{i}_1}(s)=\frac{\alpha_3}{\delta_1}$ and $G_{\hat{d}_1/\hat{i}_2}(s)=\frac{\alpha_4}{\delta_1}$ are output-to-control transfer functions; $G_{\hat{d}_2/\hat{i}_1}(s)=\frac{\beta_3}{\delta_2}$ and $G_{\hat{d}_2/\hat{i}_2}(s)=\frac{\beta_4}{\delta_2}$ are output-to-control transfer function, with

$$\alpha_1=\frac{2}{T}(K_2-K_1)\left(k_{p1}+\frac{k_{i1}}{s}\right),\alpha_2=-\frac{2}{T}(K_2-K_1)r_s,$$

$$\alpha_3=\frac{2}{T}\left\{(K_2-K_1)\left(k_{p1}+\frac{k_{i1}}{s}\right)r_{s1}+\frac{R_{d1}}{2L}\right.$$
$$[2(V_{c1}-r_sI_L)-[(K_2+K_3)D_1^2$$
$$\left.-(2K_1+4K_3)D_1+K_1-K_2+3K_3]T]\right\},$$

$$\alpha_4=\frac{R_{d2}}{TL}$$
$$\times\{2(V_{c1}-r_sI_L)-[(K_2+K_3)D_1^2-2K_3D_1+K_3]T\},$$

$$\beta_1=\frac{2}{T}(K_2+K_3)\left(k_{p2}+\frac{k_{i2}}{s}\right),\beta_2=-\frac{2}{T}(K_2+K_3)r_s,$$

$$\beta_3=\frac{R_{d1}}{L}\left[(-2K_1+K_2-K_3)D_2^2\right.$$
$$\left.+2(K_1-K_2+K_3)D_2+K_2-K_3\right],$$

$$\beta_4=\frac{R_{d2}}{L}(2K_1D_2^2-K_2D_2^2+K_3D_2^2+2K_2D_2)$$
$$-\frac{2r_{s2}}{T}(K_2+K_3)\left(k_{p2}+\frac{k_{i2}}{s}\right),$$

$$\delta_1=2(-K_1K_2D_1-K_1K_3D_1-K_2K_3D_1$$
$$-K_3^2D_1+K_1K_3+K_3^2),$$

$$\delta_2=2(K_1^2D_2-K_1K_2D_2+K_1K_3D_2$$
$$-K_2K_3D_2+K_1K_2+K_2K_3),$$

$$D_1=\frac{i_1}{i_1+i_2},D_2=\frac{i_2}{i_1+i_2}.$$

From (14) and (15), and the small signal model of the SIDO buck LED driver in Fig. 5, the block diagram of a small signal model of the PCM-controlled SIDO buck LED driver is shown in Fig. 6.

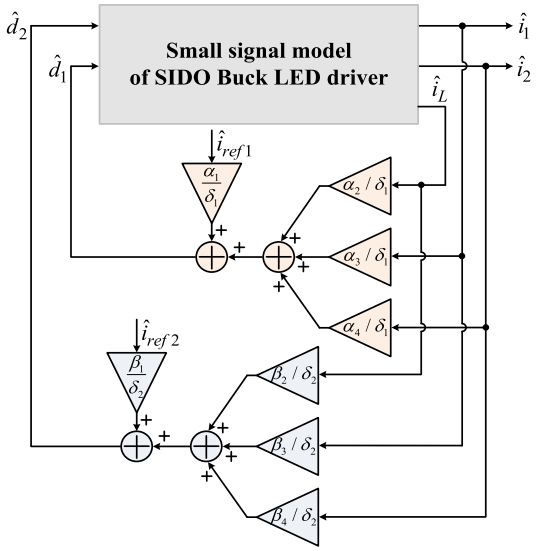

Fig. 6. Block diagram of a small signal model of the PCM-controlled SIDO buck LED driver.

C. Transfer Functions

There are two controlled switches and two outputs for the SIDO buck LED driver. According to (4) and (5), two open-loop control-to-output transfer functions of the SIDO buck LED driver can be obtained by (16a) and (16b) as given in Table I, where $G_{\hat{i}_1/\hat{d}_1}(s)$ and $G_{\hat{i}_2/\hat{d}_2}(s)$ denote the control-to-output transfer functions of output 1 and output 2, respectively. Similarly, the open-loop control-to-inductor current transfer functions can be obtained by (17a) and (17b) as given in Table I. These functions are used to design control parameters by obtaining loop gain transfer functions.

With $G_{\hat{d}_1/\hat{i}_L}(s)$, $G_{\hat{d}_2/\hat{i}_L}(s)$, $G_{\hat{d}_1/\hat{i}_1}(s)$, $G_{\hat{d}_2/\hat{i}_2}(s)$, and the transfer functions given in Table I, the block diagram of control-to-output loop gain transfer functions $T_1(s)$ of $\hat{d}_1$ to $\hat{i}_1$ and $T_2(s)$ of $\hat{d}_2$ to $\hat{i}_2$ are established, as shown in Fig. 7 and 8, respectively,

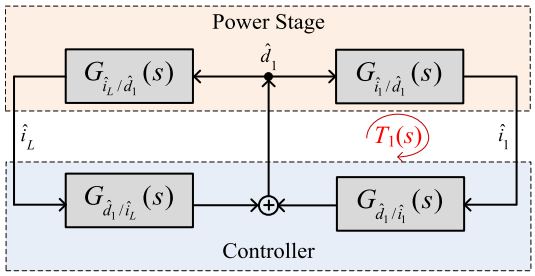

Fig. 7. Transfer function block diagram of $T_1(s)$.

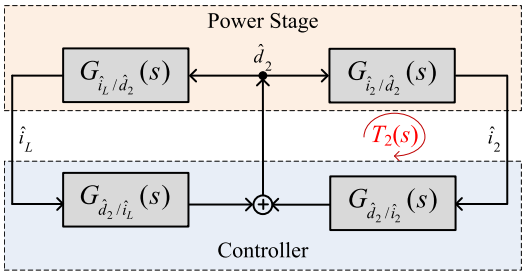

Fig. 8. Transfer function block diagram of $T_2(s)$.

which can be represented as follows:

$$T_1(s) = \frac{G_{\hat{i}_1/\hat{d}_1}(s)G_{\hat{d}_1/\hat{i}_1}(s)}{1 - G_{\hat{i}_L/\hat{d}_1}(s)G_{\hat{d}_1/\hat{i}_L}(s)} \tag{18a}$$

$$T_2(s) = \frac{G_{\hat{i}_2/\hat{d}_2}(s)G_{\hat{d}_2/\hat{i}_2}(s)}{1 - G_{\hat{i}_L/\hat{d}_2}(s)G_{\hat{d}_2/\hat{i}_L}(s)}. \tag{18b}$$

In Figs. 5 and 6, the cross-regulation transfer functions $G_{\hat{i}_1/\hat{i}_{\text{ref2}}}(s)$ and $G_{\hat{i}_2/\hat{i}_{\text{ref1}}}(s)$ of output 1 and output 2 are given in (19a) and (19b), as listed in Appendix, respectively.

Therefore, (16)–(18) serve as a basis for the design of control parameters, and (19) provides a basis for analyzing the transient cross-regulation.

D. Design of Control Parameters

In this article, LED_1 and LED_2 are selected as *XLamp MC-E white LED*. According to the *I-V* characteristic of this type of LED, forward voltages of LED_1 and LED_2 are $V_d = 2.7$ V, and equivalent resistors of LED_1 and LED_2 are $R_{d1} = 1.25\ \Omega$ and $R_{d2} = 1.5\ \Omega$ under output currents $i_1 = 600$ mA and $i_2 = 200$ mA. Table II lists the rated circuit parameters of the PCM-controlled SIDO buck LED driver.

The open-loop control-to-output transfer function of output 1 can be rewritten with $s = j\omega$, where $\omega = 2\pi f$. According to [2] and [21], the desired cross-over frequency of the LED driver is usually in the range of [1/(20T), 1/(10T)]. This article selects the desired cross-over frequency of the PCM-controlled SIDO buck LED driver as $f_c = 1/(10T) = 5$ kHz. Regarding Table II, at $f_c = 5$ kHz, the magnitude of $G_{\hat{i}_1/\hat{d}_1}(s)$ is

$$20\lg\left|G_{\hat{i}_1/\hat{d}_1}(j\omega_c)\right| = -12\ \text{dB}. \tag{20a}$$

TABLE II
PARAMETERS OF PCM-CONTROLLED SIDO BUCK LED DRIVER

Variable	Definition	Value
v_i	Rated input voltage	10 V
v_1, v_2	Rated output voltages of LED_1 and LED_2	3.45 V, 3 V
i_1, i_2	Rated output currents of LED_1 and LED_2	600 mA, 200 mA
L	Inductor	100 μH
C_1, C_2	Capacitors of output 1 and output 2	220 μF
T	Switching cycle	20 μs
V_d	Forward voltages of LED_1 and LED_2	2.7 V
R_{d1}, R_{d2}	Equivalent resistors of LED_1 and LED_2	1.25 Ω, 1.5 Ω
r_s	Sensed resistor of i_L	100 mΩ
r_{s1}, r_{s2}	Sensed resistors of i_1 and i_2	25 mΩ

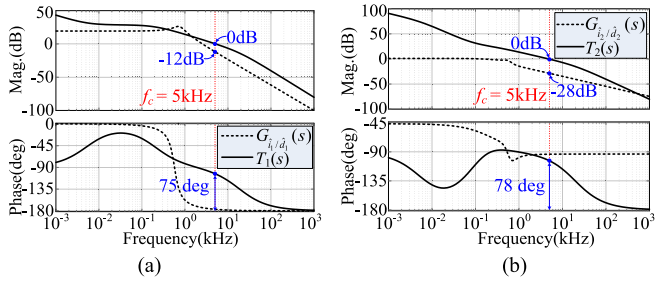

Fig. 9. Bode plots of control-to-output loop gain transfer functions. (a) $T_1(s)$. (b) $T_2(s)$.

Similarly, at $f_c = 5$ kHz, the magnitude of $G_{\hat{i}_2/\hat{d}_2}(s)$ is

$$20\lg\left|G_{\hat{i}_2/\hat{d}_2}(j\omega_c)\right| = -28\ \text{dB}. \tag{20b}$$

The results of (20) show that the studied driver is unstable.

According to (20), PCM control should compensate a gain of 12 dB for $G_{\hat{i}_1/\hat{d}_1}(j\omega_c)$ and 28 dB for $G_{\hat{i}_2/\hat{d}_2}(j\omega_c)$ of the SIDO buck LED driver to obtain a unity loop gain at $f_c = 5$ kHz. After compensation for PCM control, magnitudes of $T_1(s)$ and $T_2(s)$ are 0 dB at $f_c = 5$ kHz, which means

$$20\lg|T_1(s)| = 20\lg|T_1(j\omega_c)| = 0\ \text{dB} \tag{21a}$$

$$20\lg|T_2(s)| = 20\lg|T_2(j\omega_c)| = 0\ \text{dB}. \tag{21b}$$

According to time-domain simulation and (21), k_{i1} and k_{i2} can be calculated as $k_{i1} = 80.6$ and $k_{i2} = 833$, respectively, by choosing $k_{p1} = 1$ and $k_{p2} = 25$.

According to (16) and (18), the bode plots of the open-loop control-to-output transfer function $G_{\hat{i}_1/\hat{d}_1}(s)$ and control-to-output loop gain transfer function $T_1(s)$ are shown in Fig. 9(a). In addition, the bode plots of the open-loop control-to-output transfer function $G_{\hat{i}_2/\hat{d}_2}(s)$ and control-to-output loop gain transfer function $T_2(s)$ are shown in Fig. 9(b), where dotted lines represent amplitude-frequency and phase-frequency curves of open-loop control-to-output transfer functions, and solid lines indicate amplitude-frequency and phase-frequency curves of control-to-output loop gain transfer functions.

The system is stable if the total phase shift around the loop at the cross-over frequency f_c is less than 360 deg and larger than

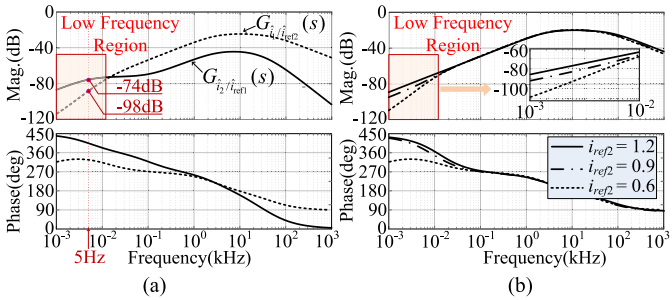

Fig. 10. Bode plots of cross-regulation transfer functions. (a) $G_{\hat{i}_1/\hat{i}_{\rm ref2}}(s)$ and $G_{\hat{i}_2/\hat{i}_{\rm ref1}}(s)$. (b) $G_{\hat{i}_1/\hat{i}_{\rm ref2}}(s)$ with different $i_{\rm ref2}$.

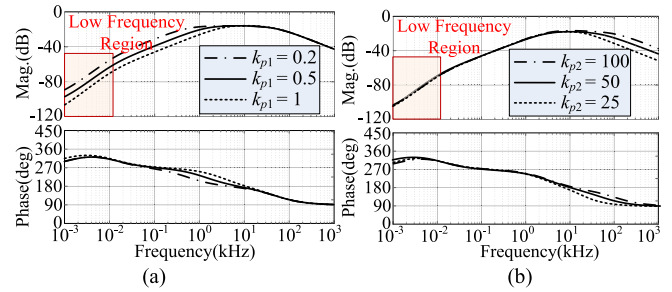

Fig. 11. Bode plots of cross-regulation transfer functions. (a) $G_{\hat{i}_1/\hat{i}_{\rm ref2}}(s)$ with different k_{p1}. (b) $G_{\hat{i}_1/\hat{i}_{\rm ref2}}(s)$ with different k_{p2}.

45 deg. It can be seen in Fig. 9(a) and (b) that the magnitudes of $G_{\hat{i}_1/\hat{d}_1}(s)$ and $G_{\hat{i}_2/\hat{d}_2}(s)$ are -12 and -28 dB, and the magnitudes of $T_1(s)$ and $T_2(s)$ are 0 dB at $f_c = 5$ kHz, which are corresponding to (20) and (21), respectively. Additionally, the phase margins of $T_1(s)$ and $T_2(s)$ are 75 deg and 78 deg at $f_c =$ 5 kHz, respectively, indicating that the PCM-controlled SIDO buck LED driver with the designed control parameters is stable.

E. Transient Cross-Regulation Analysis

Transient cross-regulation of the proposed PCM-controlled SIDO buck LED driver is investigated with bode plots based on the established small signal model presented in Fig. 6. With control parameters and circuit parameters listed in Table II, the bode plots of $G_{\hat{i}_1/\hat{i}_{\rm ref2}}(s)$ and $G_{\hat{i}_2/\hat{i}_{\rm ref1}}(s)$ are given in Fig. 10(a), in which the dotted lines and solid lines denote the amplitude-frequency and phase-frequency curves of $G_{\hat{i}_1/\hat{i}_{\rm ref2}}(s)$ and $G_{\hat{i}_2/\hat{i}_{\rm ref1}}(s)$ in the frequency domain, respectively. As can be seen in Fig. 10(a), the low-frequency gain of $G_{\hat{i}_1/\hat{i}_{\rm ref2}}(s)$ and $G_{\hat{i}_2/\hat{i}_{\rm ref1}}(s)$ are -98 and -74 dB at $f = 5$ Hz, respectively. These results are consistent with analysis results, which are calculated as $20\lg|G_{\hat{i}_1/\hat{i}_{\rm ref2}}(j\omega)| = -98$ dB and $20\lg|G_{\hat{i}_2/\hat{i}_{\rm ref1}}(j\omega)| = -74$ dB.

Furthermore, the bode plots of $G_{\hat{i}_1/\hat{i}_{\rm ref2}}(s)$ with $i_{\rm ref2} = 1.2$, 0.9, and 0.6, corresponding to $i_2 = 400$, 300, and 200 mA, respectively, are given in Fig. 10(b). As shown in Fig. 10(b), smaller $i_{\rm ref2}$ corresponds to smaller low-frequency gain. It indicates that a smaller transient cross-regulation is generated from output 2 to output 1.

The bode plots of $G_{\hat{i}_1/\hat{i}_{\rm ref2}}(s)$ with different k_{p1} ($k_{p1} = 0.2$, 0.5, and 1) are given in Fig. 11(a). As shown in Fig. 11(a), the larger the k_{p1}, the smaller the low-frequency gain in the bode plot. It means that a smaller transient cross-regulation is generated from output 2 to output 1.

Similarly, the bode plots of $G_{\hat{i}_1/\hat{i}_{\rm ref2}}(s)$ with different k_{p2} ($k_{p2} = 25$, 50, and 100) are given in Fig. 11(b). As shown in Fig. 11(b), the low-frequency gains of $G_{\hat{i}_1/\hat{i}_{\rm ref2}}(s)$ are almost the same with different k_{p2}, which means that k_{p2} does not affect the transient cross-regulation of the LED driver.

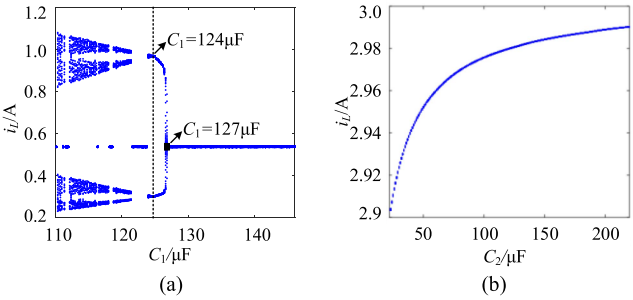

Fig. 12. Bifurcation diagram of i_L with respect to capacitor parameters. (a) $C_1 \in$ [110 μF, 146 μF]. (b) $C_2 \in$ [22 μF, 220 μF].

F. Effect of Capacitor Parameters on Stability

According to the stability analysis method in [22] and [23], the bifurcation diagrams of i_L versus capacitor parameters C_1 and C_2 are given in Fig. 12.

In Fig. 12(a), when C_1 varies from 110 to 146 μF, the stable range of C_1 is from 127 to 146 μF. In the case of 124 μF $< C_1 <$ 127 μF, the period-2 is presented. In the case of 110 μF $< C_1 <$ 124 μF, the multiple-period and chaos occur. The period-2, multiple-period, and chaos are unstable phenomena. Thus, to guarantee the stability of the studied LED driver, the minimum value of C_1 is 127 μF, and other circuit parameters have rated values. In Fig. 12(b), when C_2 changes from 22 to 220 μF, the inductor current i_L is always in the period-1, presenting that C_2 has no effect on the stability of the studied LED driver.

IV. Experimental Results

A. Experiment Setup

The experimental setup is carried out in this section to verify the analysis results. The experimental hardware prototype and laboratory setup of the PCM-controlled SIDO buck LED driver is shown in Fig. 13, with the main components of the prototype are listed in Table III.

B. Experimental Verification for Operation Principle

Fig. 14 illustrates experimental waveforms of the control timing and steady-state waveforms of input voltage and output currents.

In Fig. 14(a), the waveforms from top to bottom are inductor current i_L, clock signal clk, control signal V_{g2} of S_2, and control signal V_{g1} of S_1. When clk is triggered in a switching cycle, V_{g1} and V_{g2} have high levels, and i_L increases. Then, V_{g2} has a low level, and i_L increases. Finally, V_{g1} has a low level, and i_L decreases. This corresponds to the theoretical analysis.

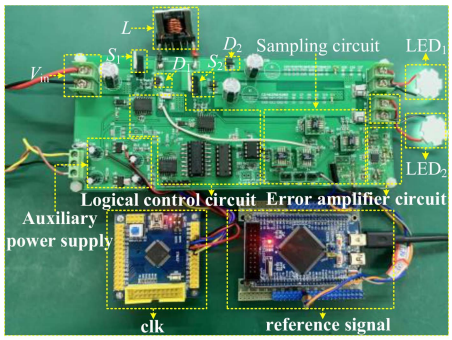

(a)

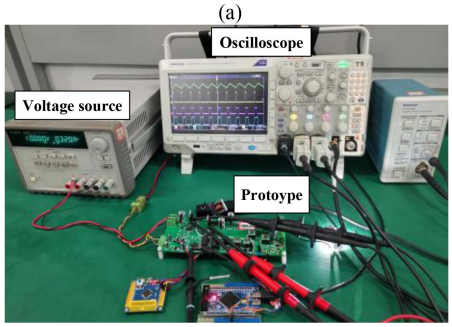

(b)

Fig. 13. Photographs of experimental hardware prototype and laboratory setup of the proposed converter. (a) Hardware prototype. (b) Laboratory setup.

TABLE III
MAIN COMPONENTS ADOPTED IN HARDWARE PROTOTYPE

Components	Type
MOSFET switches	IRFB4110, IRF540N
MOSFET drivers	IR2110S
Diodes	SS54
Comparators	LM393
Amplifiers	LT1357, OPA2347
RS triggers	CD4043
AND gate	HD74LS08P
Signal isolator	ISO7240
Reference signal controller	STM32F103ZET6
Clock signal controller	STM32F103C8T6
Auxiliary power supply	LM317, LM337

In Fig. 14(b), the waveforms from top to bottom are output currents i_1, i_2, and input voltage v_i, which are zoomed by a separate picture with a time scale of 100 μs. It can be seen when $v_i = 10$ V, $i_1 = 600$ mA, and $i_2 = 200$ mA, which agree with the rated parameters. The current ripples of i_1 and i_2 are $\Delta i_1 = 40$ mA and $\Delta i_2 = 20$ mA, respectively.

Similarly, Fig. 14(c) shows the waveforms with $v_i = 10$ V, $i_1 = 600$ mA, and $i_2 = 500$ mA, in which i_2 is close to i_1. The current ripples of i_1 and i_2 are $\Delta i_1 = 30$ mA and $\Delta i_2 = 30$ mA, respectively. The experimental results verify the analysis results of the operation principle of SIDO topology.

C. Experimental Verification for PCM Control

In this subsection, experimental transient waveforms of the PCM-controlled SIDO buck LED driver are presented to verify

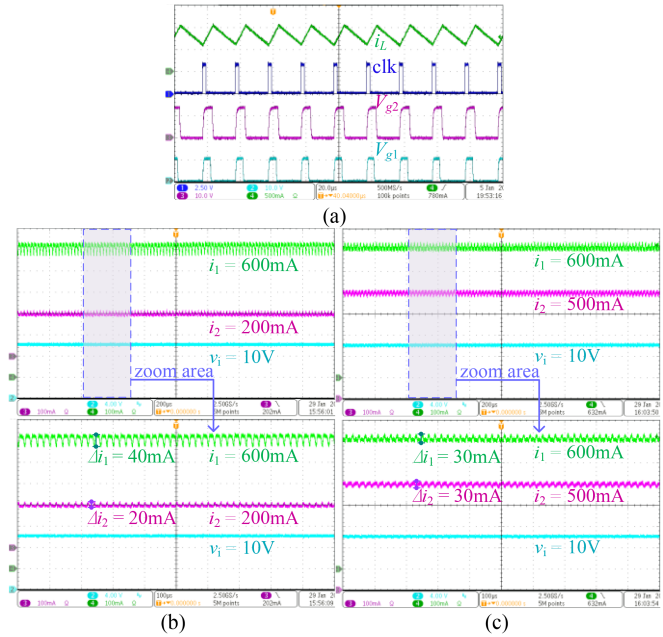

(a) (b) (c)

Fig. 14. Experimental steady-state waveforms of the PCM-controlled SIDO buck LED driver. (a) Control timing. (b) Input voltage and output currents ($i_1 = 600$ mA, $i_2 = 200$ mA). (c) Input voltage and output currents ($i_1 = 600$ mA, $i_2 = 500$ mA).

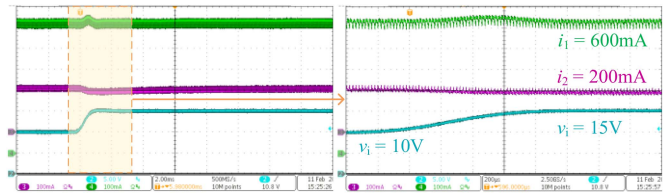

Fig. 15. Experimental transient waveforms of i_1 and i_2 with variation of input voltage.

the validity of the PCM control. Fig. 15 shows experimental results when v_i step increases from 10 to 15 V. It can be known that output currents i_1 and i_2 can maintain constant currents of 600 and 200 mA after an adjustment period, respectively. Thus, the LED driver achieves constant output currents.

Fig. 16(a) and (b) present experimental results when the reference signal of i_{ref2} step increases from 0.3 to 0.6, and step decreases from 0.6 to 0.3, corresponding to 100 to 200 mA load interchange of output currents i_2. Reference signal i_{ref1} remains constant. As shown in Fig. 16, output current i_2 changes from 100 to 200 mA and then returns to 100 mA, while output current i_1 remains 600 mA. This verifies the precise and independent dimming capability of the LED driver.

D. Experimental Verification for Transient Cross-Regulation Analysis

Fig. 17(a)–(c) show experimental results when the reference signal i_{ref2} step decreases from 1.2 to 0.6 ($i_2 = 400$ mA→200 mA), from 0.9 to 0.45 ($i_2 = 300$ mA→150 mA), and from 0.6 to 0.3 ($i_2 = 200$ mA→100 mA), while reference signal i_{ref1} keeps constant, corresponding to 100% to 50% load interchange,

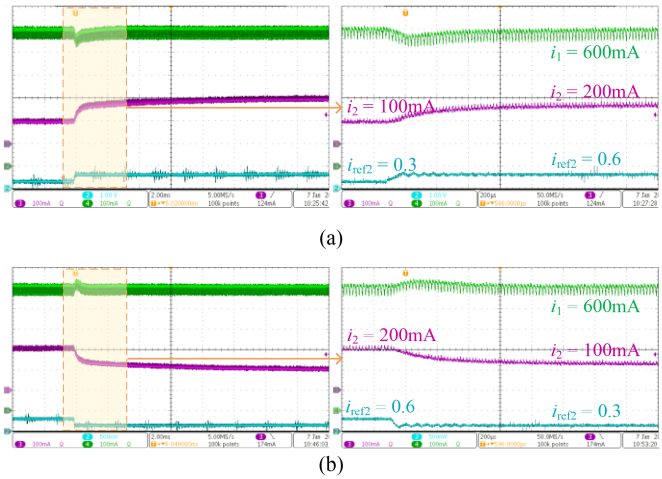

Fig. 16. Experimental transient waveforms of i_1 and i_2 with variation of reference signal $i_{\rm ref2}$. (a) $i_{\rm ref2} = 0.3 \rightarrow 0.6$. (b) $i_{\rm ref2} = 0.6 \rightarrow 0.3$.

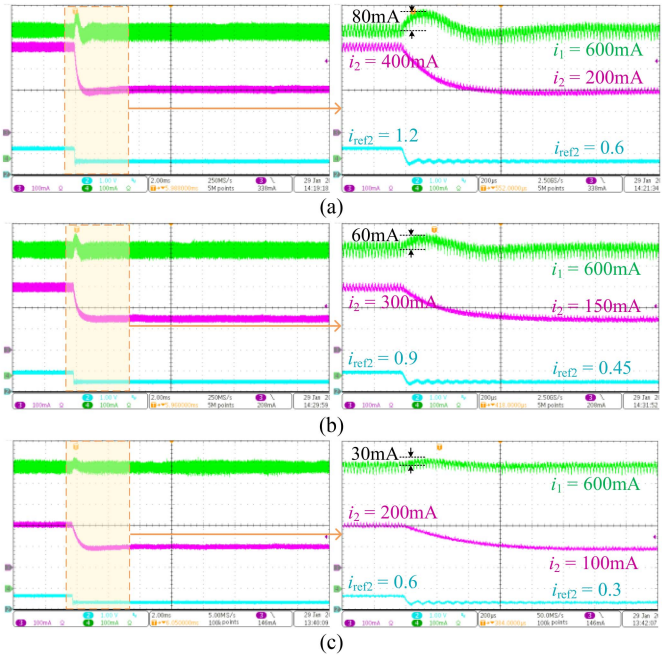

Fig. 17. Output currents waveforms with variation of reference signal $i_{\rm ref2}$. (a) $i_{\rm ref2} = 1.2 \rightarrow 0.6$. (b) $i_{\rm ref2} = 0.9 \rightarrow 0.45$. (c) $i_{\rm ref2} = 0.6 \rightarrow 0.3$.

respectively. Fig. 17 shows that the transient cross-regulation from output 2 to output 1 in these three cases are 80, 60, and 30 mA, respectively, meaning that reducing $i_{\rm ref2}$ will decrease transient cross-regulation from output 2 to output 1 when the same load variation occurs in output 2.

Fig. 18(a) and (b) show experimental results when the reference signal $i_{\rm ref2}$ step decreases from 0.6 to 0.3 (i_2 = 200 mA→100 mA), while $k_{p1} = 0.2$ and 0.5, respectively. Combined with Fig. 17(c) ($k_{p1} = 1$), it can be observed that the transient cross-regulations from output 2 to output 1 are 50, 40, and 30 mA, respectively.

Fig. 19 shows experimental results when the reference signal $i_{\rm ref2}$ step decreases from 0.6 to 0.3 (i_2 = 200 mA→100 mA),

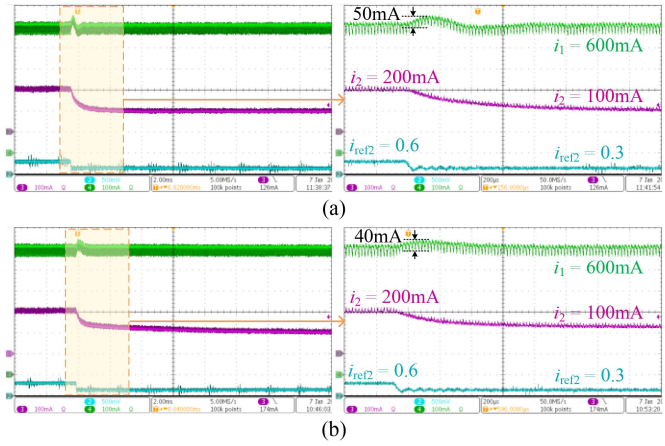

Fig. 18. Output currents waveforms with different k_{p1}. (a) $k_{p1} = 0.2$. (b) $k_{p1} = 0.5$.

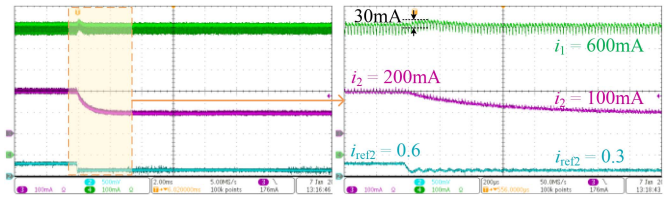

Fig. 19. Output currents waveforms with $k_{p2} = 50$.

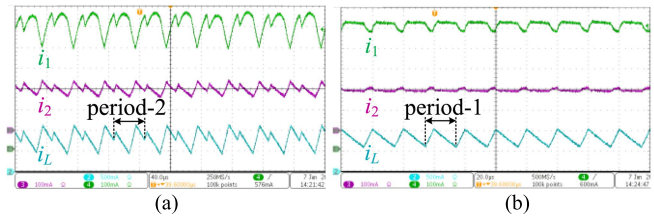

Fig. 20. Experimental steady-state waveforms of output currents and inductor current with different C_1. (a) $C_1 = 125\ \mu$F. (b) $C_1 = 220\ \mu$F.

while $k_{p2} = 50$. Combined with Fig. 17(c) ($k_{p2} = 25$), transient cross-regulations from output 2 to output 1 are almost the same.

The above experimental results verify the transient cross-regulation analysis results in Section IV.

E. Experimental Verification for Stability Analysis of C_1

The experimental steady-state waveforms of output currents i_1, i_2, and inductor current i_L of the PCM-controlled SIDO buck LED driver with different C_1 are presented in Fig. 20. As can be seen in Fig. 20(a), when $C_1 = 125\ \mu$F, the i_1, i_2, and i_L are in period-2. While the i_1, i_2, and i_L are in stable period-1 with $C_1 = 220\ \mu$F in Fig. 20(b). These results confirm the analytical result regarding the effect of C_1 on the stability of the studied LED driver.

F. Measured Efficiency and Comparison Analysis

Fig. 21 shows measured efficiency versus the output power. It can be seen that as the output power increases, the efficiency

$$G_{\hat{i}_1/\hat{i}_{\mathrm{ref2}}}\big|_{\hat{i}_{\mathrm{ref1}}=0} = \frac{-\mathrm{SL}\beta_1\left\{\alpha_2\mathrm{V_i}\left(1-\mathrm{D_2}\right)\left(\mathrm{V_1}-\mathrm{V_2}\right)-\left(\alpha_2\mathrm{V_i}-\mathrm{SL}\delta_1\right)\left[\left(1-\mathrm{D_2}\right)\left(\mathrm{V_1}-\mathrm{V_2}\right)-\mathrm{SLI_L}\right]\right\}}{\left[\mathrm{SL}\beta_3-\mathrm{R}_{d1}\beta_2\left(1-\mathrm{D_2}\right)\right]\left\{\alpha_2\mathrm{V_i}\left(1-\mathrm{D_2}\right)\left(\mathrm{V_1}-\mathrm{V_2}\right)-\left(\alpha_2\mathrm{V_i}-\mathrm{SL}\delta_1\right)\left[\left(1-\mathrm{D_2}\right)\left(\mathrm{V_1}-\mathrm{V_2}\right)-\mathrm{SLI_L}\right]\right\}} + \beta_2\mathrm{V_i}\left\{\left[\left(1-\mathrm{D_2}\right)\left(\mathrm{V_1}-\mathrm{V_2}\right)-\mathrm{SLI_L}\right]\left[\mathrm{SL}\alpha_3-\mathrm{R}_{d1}\alpha_2\left(1-\mathrm{D_2}\right)\right]+\alpha_2\left(\mathrm{V_1}-\mathrm{V_2}\right)\left[\mathrm{SL}+\mathrm{R}_{d1}(1-\mathrm{D_2})^2\right]\right\} + \left[\beta_2\left(\mathrm{V_1}-\mathrm{V_2}\right)-\mathrm{SL}\delta_2\right]\left\{\mathrm{R}_{d1}\alpha_2\mathrm{V_i}(1-\mathrm{D_2})^2-\mathrm{SL}\alpha_3\mathrm{V_i}\left(1-\mathrm{D_2}\right)-\left(\alpha_2\mathrm{V_i}-\mathrm{SL}\delta_1\right)\left[\mathrm{SL}+\mathrm{R}_{d1}(1-\mathrm{D_2})^2\right]\right\} \tag{19a}$$

$$G_{\hat{i}_2/\hat{i}_{\mathrm{ref1}}}\big|_{\hat{i}_{ref2}=0} = \frac{-\mathrm{SL}\alpha_1\mathrm{V_i}\left\{\mathrm{D_2}\left[\beta_2\left(\mathrm{V_1}-\mathrm{V_2}\right)-\mathrm{SL}\delta_2\right]-\beta_2\left[\mathrm{D_2}\left(\mathrm{V_1}-\mathrm{V_2}\right)+\mathrm{SLI_L}\right]\right\}}{\left(\alpha_2\mathrm{V_i}-\mathrm{SL}\delta_1\right)\left\{\left(\mathrm{SL}\beta_4-\mathrm{R_{d2}D_2}\beta_2\right)\left[\mathrm{D_2}\left(\mathrm{V_1}-\mathrm{V_2}\right)+SLI_L\right]+\left(\mathrm{R}_{d2}\mathrm{D_2^2}+\mathrm{SL}\right)\left[\beta_2\left(\mathrm{V_1}-\mathrm{V_2}\right)-\mathrm{SL}\delta_2\right]\right\} + \mathrm{V}_i\left(\mathrm{SL}\alpha_4-\mathrm{R}_{d2}\mathrm{D_2}\alpha_2\right)\left\{\mathrm{D_2}\left[\beta_2\left(\mathrm{V_1}-\mathrm{V_2}\right)-\mathrm{SL}\delta_2\right]-\beta_2\left[\mathrm{D_2}\left(\mathrm{V_1}-\mathrm{V_2}\right)+\mathrm{SLI}_L\right]\right\} - SL\alpha_2\mathrm{V}_i\left(\mathrm{V_1}-\mathrm{V_2}\right)\left(D_2\beta_4+\beta_2\right). \tag{19b}$$

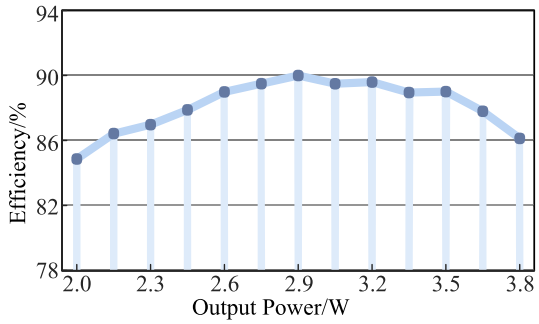

Fig. 21. Measured efficiency versus the output power.

TABLE IV
PROPOSED METHOD CHARACTERISTICS COMPARED WITH EXISTING METHODS

Description	Ref. [1]	Ref. [2]	Ref. [12]	This work
LED	Three channels	Three channels	Four channels	Two channels
Mode	DCM	DCM	CCM	CCM
Control method	AC-TM	VM-TM	ACC-TM	PCM
Dimming type	Sequential	Individual	Individual	Individual
Steady-state cross-regulation	≤2%	0	≤1%	0
Output current ripple factor	/	12%	14%	≤10%
Maximum efficiency	90%	89%	96%	90%

of the proposed SIDO LED driver increases first and then decreases. The maximum efficiency is 90% at output power of 2.9 W.

Table IV presents a comparison of the proposed SIDO LED driver with the state-of-the-art. The results demonstrate that the proposed SIDO LED driver has a lower output current ripple factor than that of [2] and [12]. In addition, the steady-state cross-regulation in [1] and [12] are less than 2% and 1%, respectively, while the proposed SIDO LED driver has no steady-state cross-regulation with individual PCM control. Furthermore, the proposed method exhibits higher efficiency compared to the existing methods in [2].

V. CONCLUSION

In this article, a PCM-controlled SIDO buck LED driver was proposed to achieve independent current control of each LED output. It had no steady-state cross-regulation. A small signal model of the LED driver was established based on the inductor current ripple by state-space average modeling approach to design suitable control parameters and to investigate the transient cross-regulation. The bode plots of control-to-output loop gain transfer functions showed that the PCM-controlled SIDO buck LED driver is stable with designed control parameters. The bode plots of cross-regulation transfer functions proved that reducing the reference signal of one output and increasing control parameter k_{p1} decreases transient cross-regulation from one output to the other. Besides, the effect of the capacitor on the stability of the studied LED driver is investigated using bifurcation analysis. In addition, experimental results demonstrated these theoretical studies. In addition, the PCM control can be extended to other SIDO or SIMO LED drivers. It should be noted that the small signal modeling, control parameters design, and transient cross-regulation analysis methods presented in this article provided a theoretical reference to other ripple-based controlled SIDO or SIMO LED drivers.

APPENDIX

Equation (19a) and (19b) shown at the top of this page.

REFERENCES

[1] H. Chen, Y. Zhang, and D. S. Ma, "A SIMO parallel-string driver IC for dimmable led backlighting with local bus voltage optimization and single time-shared regulation loop," *IEEE Trans. Power Electron.*, vol. 27, no. 1, pp. 452–462, Jan. 2012.

[2] Y. Guo, S. Li, A. T. L. Lee, S. -C. Tan, C. K. Lee, and S. Y. R. Hui, "Single-stage AC/DC single-inductor multiple-output LED drivers," *IEEE Trans. Power Electron.*, vol. 31, no. 8, pp. 5837–5850, Aug. 2016.

[3] D. Gacio, J. M. Alonso, J. Garcia, L. Campa, M. J. Crespo, and M. Rico-Secades, "PWM series dimming for slow-dynamics HPF LED drivers: The high-frequency approach," *IEEE Trans. Ind. Electron.*, vol. 59, no. 4, pp. 1717–1727, Apr. 2012.

[4] S. N. Li, Y. Guo, S. C. Tan, and S. Y. Hui, "An off-line single-inductor multiple-output LED driver with high dimming precision and full dimming range," *IEEE Trans. Power Electron.*, vol. 32, no. 6, pp. 4716–4727, Jun. 2017.

[5] M. Tahan and T. Hu, "Multiple string LED driver with flexible and high performance PWM dimming control," *IEEE Trans. Power Electron.*, vol. 32, no. 12, pp. 9293–9306, Dec. 2017.

[6] K. Modepalli and L. Parsa, "A scalable N-color LED driver using single inductor multiple current output topology," *IEEE Trans. Power Electron.*, vol. 31, no. 5, pp. 3773–3783, May 2016.
[7] S. Dietrich, S. Strache, R. Wunderlich, and S. Heinen, "Get the LED out: Experimental validation of a capacitor-free single-inductor multiple-output LED driver topology," *IEEE Ind. Electron. Mag.*, vol. 9, no. 2, pp. 24–35, Jun. 2015.
[8] A. T. L. Lee, J. K. O. Sin, and P. C. H. Chan, "Scalability of quasi-hysteretic FSM-based digitally controlled single-inductor dual-string buck LED driver to multiple strings," *IEEE Trans. Power Electron.*, vol. 29, no. 1, pp. 501–513, Jan. 2014.
[9] Y. Wang, J. P. Xu, and G. Yin, "Cross-regulation suppression and stability analysis of capacitor current ripple controlled SIDO CCM buck converter," *IEEE Trans. Ind. Electron.*, vol. 66, no. 3, pp. 1770–1780, Mar. 2019.
[10] D. S. Ma, W. H. Ki, and C. Y. Tsui, "A pseudo-CCM/DCM SIMO switching converter with freewheel switching," *IEEE J. Solid-State Circuits*, vol. 38, no. 6, pp. 1007–1014, Jun. 2003.
[11] S. Dietrich, S. Strache, R. Wunderlich, and S. Heinen, "An innovative integration technique of a capacitor-free single-inductor multiple-output LED driver," *IEEE Ind. Electron. Mag.*, vol. 9, no. 2, pp. 50–53, Jun. 2015.
[12] W.-H. Yang, H.-A. Yang, C.-J. Huang, K.-H. Chen, and Y.-H. Lin, "A High-efficiency single-inductor multiple-output buck-type LED driver with average current correction technique," *IEEE Trans. Power Electron.*, vol. 33, no. 4, pp. 3375–3513, Apr. 2018.
[13] H. C. kim, C. S. Yoon, D. K. Jeong, and J. kim, "A single-inductor multiple-channel current-balancing LED driver for display backlight applications," *IEEE Trans. Ind. Appl.*, vol. 50, no. 6, pp. 4077–4081, Nov./Dec. 2014.
[14] Z. Dong, C. K. Tse, and S. Y. R. Hui, "Current-source-mode single-inductor multiple-output LED driver with single closed-loop control achieving independent dimming function," *IEEE J. Emerg. Select Topics Power Electron.*, vol. 6, no. 3, pp. 1198–1209, Sep. 2018.
[15] D. Trevisan, P. Mattavelli, and P. Tenti, "Digital control of single-inductor multiple-output step-down DC-DC converters in CCM," *IEEE Trans. Ind. Electron.*, vol. 55, no. 9, pp. 3476–3483, Sep. 2008.
[16] B. Chen and L. Chang-Chien, "Digitally controlled low cross-regulation single-inductor dual-output (SIDO) buck converter," in *Proc. IEEE Int. Symp. Circuits Syst.*, Jul. 2015, pp. 2497–2500.
[17] W. W. Xu, Y. Li, Z. L. Hong, and D. Killat, "A dual-mode single-inductor dual-output switching converter with small ripple," *IEEE Trans. Power Electron.*, vol. 25, no. 3, pp. 614–623, Mar. 2010.
[18] Y. Wang, J. P. Xu, and G. H. Zhou, "A cross regulation analysis for single-inductor dual-output CCM buck converters," *J. Power Electron.*, vol. 16, no. 5, pp. 1802–1812, Sep. 2016.
[19] W. Sun, C. Han, M. Yang, S. Xu, and S. Lu, "A ripple control dual-mode single-inductor dual-output buck converter with fast transient response," *IEEE Trans. Very Large Scale Integr. Syst.*, vol. 23, no. 1, pp. 107–117, Jan. 2015.
[20] S. H. Zhou, G. H. Zhou, G. Liu, and G. H. Mao, "Small-signal modeling and cross-regulation suppressing for current-mode controlled single-inductor dual-output DC-DC converters," *IEEE Trans. Ind. Electron.*, vol. 68, no. 7, pp. 5744–5755, Jul. 2021.
[21] R. W. Erickson and D. Maksimovic, *Fundamentals of Power Electronics*, 2nd ed. New York, NY, USA: Springer, 2001.
[22] A. E. Aroudi, M. Debbat, and L. Martinez-Salamero, "Poincaré mapsmodeling and local orbital stability analysis of discontinuous piecewise affine periodically driven systems," *Nonlinear Dyn.*, vol. 50, no. 3, pp. 431–445, Oct. 2007.
[23] Y. Wang, L. M. Xu, L. Chen, and J. C. Zhou, "Discrete iterative map model-based stability analysis of capacitor current ripple controlled SIDO CCM buck converter," *IEEE J. Emerg. Sel. Topics Power Electron.*, vol. 8, no. 4, pp. 3272–3280, Dec. 2020.

Yao Wang was born in Sichuan, China, in 1987. She received the B.S. degree in electrical engineering and automation from the Sichuan Normal University, Chengdu, China, in 2011, and the M.S. and Ph.D. degrees in electrical engineering from the Southwest Jiaotong University, Chengdu, China, in 2014 and 2020, respectively.

From 2014 to 2018, she was an Experimentalist and a Senior Experimentalist with the School of Electrical Engineering, Southwest Minzu University, Chengdu, China, where she has been an Associate Professor since 2023. Her research interests include the modeling, analysis, and control of power electronic systems.

Jianping Xu (Member, IEEE) received the B.S. and Ph.D. degrees in electronic engineering from the University of Electronics Science and Technology of China, Chengdu, China, in 1984 and 1989, respectively.

Since 1989, he has been with the School of Electrical Engineering, Southwest Jiaotong University, Chengdu, China, where he has been a Professor since 1995. From November 1991 to February 1993, he was with the Department of Electrical Engineering, University of Federal Defense Munich, Munich, Germany, as a Visiting Research Fellow. From February 1993 to July 1994, he was with the Department of Electrical Engineering and Computer Science, University of Illinois at Chicago, Chicago, IL, USA, as a Visiting Scholar. He has authored or coauthored more than 400 technical papers. His research interests include the modeling and control of power electronic systems, high-efficiency/high-power density power converters, and wireless power transfer system.

Zhangyong Chen was born in Sichuan, China, in 1988. He received the B.S. degree in electrical engineering and its automation, and the Ph.D. degree in electrical engineering from the Southwest Jiaotong University, Chengdu, China, in 2010 and 2015, respectively.

From 2014 to 2015, he was a Visiting Student with the Future Energy Electronics Center, Virginia Tech, Blacksburg, VA, USA. Since January 2016, he has been a Lecturer with the School of Energy Science and Engineering and from Jul. 2018, he was been an Associate Professor with the School of Automation Engineering, University of Electronic Science and Technology of China, Chengdu, China. His research interests include switching-mode power supplies, soft-switching techniques, power factor correction converters, and renewable energy sources.

Fuban Qin was born in Guangxi, China, in 1993. He received the B.S. degree in electrical engineering and automation from the Southwest Minzu University, Chengdu, China, in 2016, and the M.S. degree in electrical engineering from the Southwest Jiaotong University, Chengdu, China, in 2019.

In 2019, he joined in TI and became an anolog IC test ENGer. His research interests include the electronics design, coding, analysis, and control of power electronic systems.